Journal of the European Ceramic Society **12** (1993) 479–485

Interfacial Characterisation of Al_2O_3–Ni Composites

L. Chang,* S. C. Chen

Materials Research Laboratory, Industrial Tech. Research Institute, Chutung, Hsinchu, Taiwan 31015

W. H. Tuan‡

Institute of Material Science & Engineering, National Taiwan University, Taipei, Taiwan 10764

&

R. J. Brook

Department of Materials, University of Oxford, Parks Road, Oxford, OX1 3PH, UK

(Received 15 March 1993; accepted 15 June 1993)

Abstract

In the present study, the interfacial structure of nickel particle-reinforced alumina composites prepared by a gas reduction process and by reactive sintering is examined by analytical electron microscopy. Amorphous carbon films at the interface and graphite inclusions within the nickel inclusions can be found in products from gas reduction and from reaction sintering, respectively. The microstructural variation results in different amounts of toughness enhancement. Possible explanations for the resulting microstructure and toughness differences are proposed.

In der vorliegenden Arbeit wurde die Grenzflächenstruktur des Verbundwerkstoffes Aluminiumoxid verstärkt mit Nickelteilchen mit Hilfe der analytischen Elektronenmikroskopie untersucht. Die Herstellung des Verbundwerkstoffes erfolgte durch Gasreduktion und reaktives Sintern. In Proben, hergestellt durch Gasreduktion, konnten amorphe Kohlenstoffilme an der Grenzfläche nachgewiesen werden, bzw. Kohlenstoffeinschlüsse in den Nickelteilchen in Proben, die durch reaktives Sintern hergestellt wurden. Die Unterschiede im Gefüge resultieren in verschiedenen Zähigkeitszunahmen. Es werden mögliche Erklärungen für die sich ergebenden Unterschiede im Gefüge und der Zähigkeit vorgeschlagen.

Dans cette étude, les auteurs examinent par microscopie électronique analytique la structure de l'interface dans des composites à matrice d'alumine renforcée par des particules de nickel, préparés par un procédé de réduction en phase gazeuse et un frittage réactif. Des films de carbone amorphe à l'interface sont détectés dans le procédé par réduction gazeuse tandis que l'on retrouve des inclusions de graphite dans les particules de nickel après frittage réactif. Cette variation microstructurale conduit à différentes augmentations de la ténacité. Des explications sont proposées quant aux différences de microstructure finale et de ténacité.

1 Introduction

The toughening of brittle materials by ductile inclusions is of considerable interest. The approach has been successfully employed in several systems.[1–5] Previous studies[5–7] have indicated that crack bridging is usually the most potent mechanism. This can be appreciated by noting that the only ductile regions which experience extensive plastic deformation are those segments that stretch between the crack surfaces in the bridging zone. The plastic dissipation in this zone can be relatively large and can provide a major increase in toughness.

In order for the ductile inclusion to be stretched between the crack surfaces, the bonding characteristics play an important role. If the ductile inclusion is weakly bonded to the matrix, the crack will propagate along the interface and the contribution from the ductility to the toughness will be negligible. If the bonding between ceramic and metal is very strong, the extent of inclusion deformation will be

* Present address: National Science Council, Taipei, Taiwan 106.
‡ To whom correspondence should be addressed.

Journal of the European Ceramic Society 0955-2219/93/$6.00

limited (i.e. a small extension or bridging capability) resulting in limited toughness increase. For bonding with intermediate strength, a fraction of the interface is debonded as the crack reaches the interface and the effective bridging length is thereby increased with improvement in the toughness. Therefore, moderately weak interfaces are expected to result in high toughness composites.

The deformation behaviour of a ductile inclusion within a brittle matrix has been investigated by Ashby and co-workers.[7,8] They conclude that if the residual stress can be ignored then the fracture toughness increase, ΔK_{IC}, contributed by the plastic deformation is

$$\Delta K_{IC} = (CFE\sigma_y d)^{0.5} \quad (1)$$

where C is a constant which depends on the interfacial strength, F the volume fraction of the inclusions, E and σ_y are the elastic modulus and yield strength of the metal, respectively, and d is the size of the inclusion. Since the interactions between the crack and metallic inclusions depend on the shape of inclusion, it is helpful[5] to introduce a shape factor, S into eqn (1). This then becomes

$$\Delta K_{IC} = (SCFE\sigma_y d)^{0.5} \quad (2)$$

The Al_2O_3–Ni system has been investigated recently by Tuan and Brook.[5,9] The composites were prepared either by using gas reduction of nickel oxide to nickel[5] or by using reactive sintering of nickel oxide and aluminium.[9] Significant improvements in toughness were reported. However, the toughness enhancement of the composites showed a strong dependence on the fabrication route. This was attributed to the variation of the interfacial structure resulting from the different processing routes.[5,9] In the present study, the characteristics of the interfaces in the Al_2O_3–Ni composites are investigated more closely.

2 Experimental

The detail of the sample preparation procedures have been reported elsewhere.[5,9] The procedures are summarised here.

For the specimens prepared by the gas reduction process, alumina (AKP-30, Sumitomo Chemical Co. Ltd, Tokyo, Japan) and 0 to 30 w/o nickel oxide (Alfa product, Johnson Matthey Co., Danvers, USA) were attrition milled together in iso-propanol for 4 h using alumina balls as grinding media. The slurry was dried in an oven at 70°C for 3 days to remove the solvent. The dried lumps were crushed by vibration and passed through a plastic sieve with aperture size of 0·112 mm. Specimens, 2 cm in diameter and 0·4–0·5 cm in height, were prepared by cold isostatic pressing at 200 MPa. The sintering was performed in a box furnace at 1700°C for 1 h. A graphite powder bed surrounded the powder compacts; this generated a reducing atmosphere during sintering (partial pressure of oxygen $\sim 10^{-15}$ atm).[10] The heating and cooling rates used were 5°C/min.

For the specimens prepared by the reactive sintering of aluminium and nickel oxide, coarse alumina powder (F500, H.C. Stark, Berlin, Germany), aluminium droplets (ECKA AS081, ECKART-WERKE, Fuerth/Bay, Germany) and nickel oxide were attrition milled together. Two compositions, B1 and B2, were made (B1 = 14·5 w/o Al, 60·1 w/o NiO and 25·4 w/o Al_2O_3; B2 = 14·5 w/o Al, 29·1 w/o NiO and 56·4 w/o Al_2O_3). Excess alumina in B2 was used to act as a diluent to the reaction between aluminium and nickel oxide. The B2 composition resulted in 11 v/o nickel after the reaction sintering. The sample preparation and the sintering procedures were the same as those for samples made by the gas reduction process.

Polished surfaces were prepared by cutting the samples along the axial direction of the discs and polishing with diamond paste to 1 μm. Indentation was performed on a Zwick microhardness tester with a Vickers diamond indenter and a 50 N load. The relationship proposed by Lawn *et al.*[11] was used to calculate the fracture toughness.

For the analytical electron microscopy examination, thin foil specimens were prepared by slicing the sintered specimens into layers 0·5 mm thick, followed by ultrasonic cutting to 3 mm diameter discs, grinding to 50 μm thick, and dimpling to

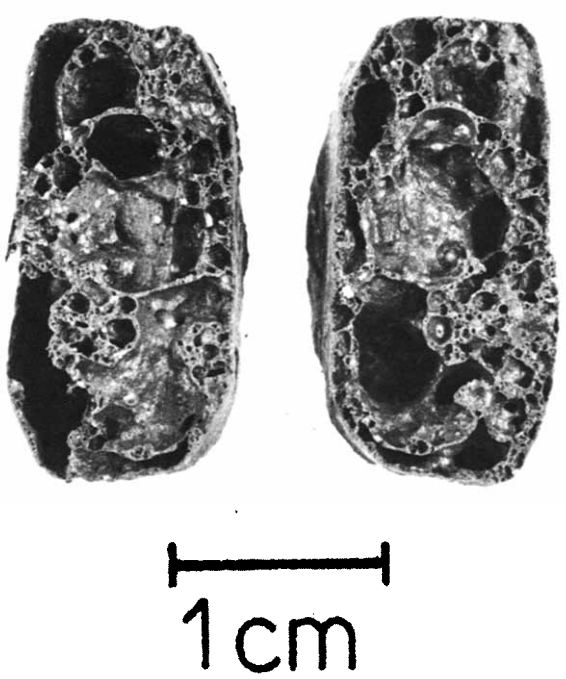

Fig. 1. The fracture surface of the composite with the composition B1 after sintering at 1700°C for 1 h.

Table 1. The relative density, toughness, K_{IC}, toughness increase, ΔK_{IC}, shape factor,[5,9] S, volume fraction, F, elastic modulus,[5] E, yield strength,[5] σ_y and inclusion size, d, of the composites prepared by the reactive sintering and the gas reduction processes

Process	*Density (%)*	K_{IC} — $(MPa\sqrt{m})$	ΔK_{IC} — $(MPa\sqrt{m})$	$S^{5,9}$	F	E^5 (GPa)	$\sigma_y{}^5$ (MPa)	d (μm)
Reactive sintering B2	98	3·6	0·9	0·37	0·11	200	320	1·6
Gas reduction	95	5·0	2·3	0·37	0·13	200	320	1·1

20 μm. Electron transparency was obtained by ion milling at 6 kV. The thin foils were then examined in an analytical electron microscope, equipped with a Link LZ5 X-ray dispersive spectrometer (EDS) and a Gatan 667 paralleled electron loss spectrometer (EELS).

3 Results

The specimen with the composition B1 after reactive sintering at 1700°C for 1 h is shown in Fig. 1. A sponge structure with huge pores resulted from the violent reaction between the aluminium and nickel oxide particles ($2Al + 3NiO = Al_2O_3 + 3Ni$). With its excess diluent of alumina, the composite B2 can be sintered to 98% of the theoretical density (Table 1). Only the properties of the B2 composition are reported in the following paragraphs.

The inclusion size of nickel in the composites is shown as a function of nickel content in Fig. 2. Typical microstructures obtained for both processes are shown in Fig. 3. The nickel particles are well distributed within the alumina matrix. The fracture toughness of the composite is shown as a function of nickel content in Fig. 4. The toughness enhancement shows strong dependence on the processing con-

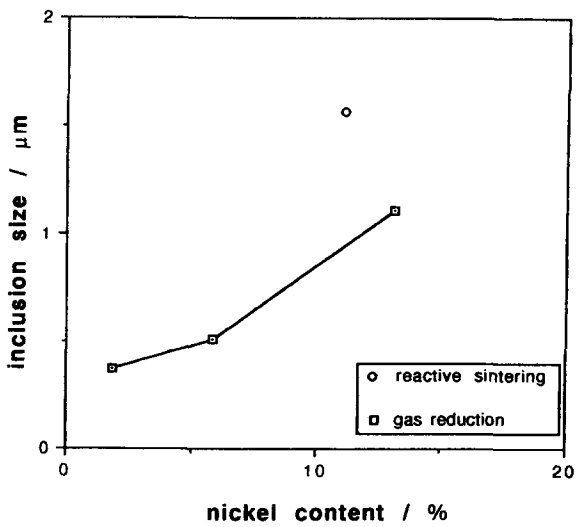

Fig. 2. The size of nickel particles of the composites as a function of nickel content. The samples are sintered at 1700°C for 1 h.

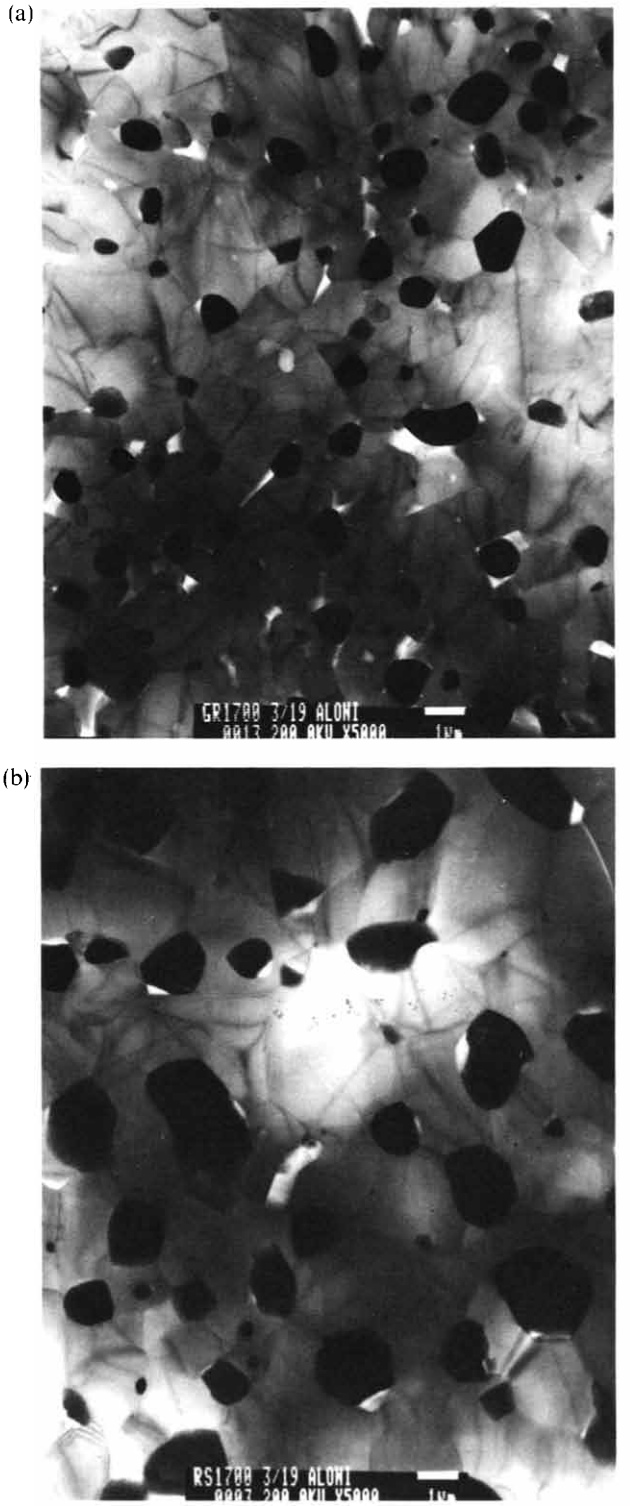

Fig. 3. TEM micrographs for the composites prepared by (a) the gas reduction, and (b) the reactive sintering processes.

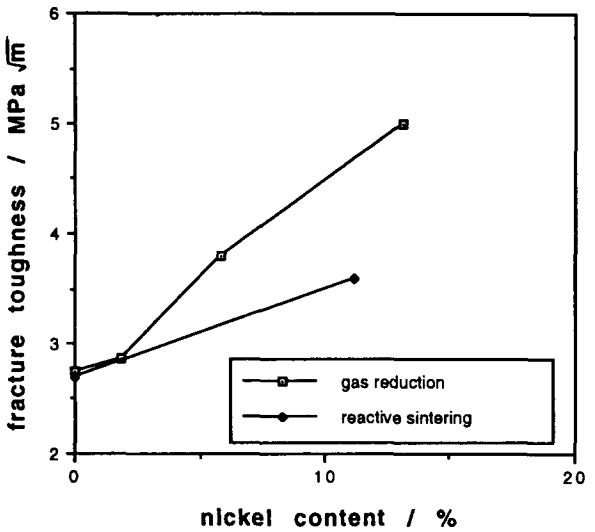

Fig. 4. The fracture toughness determined by the indentation technique for the composites shown in Fig. 2 as a function of nickel content.

ditions employed. A typical stretched nickel particle is shown in Fig. 5. Partial debonding between the interface of alumina and nickel can be observed.

In samples sintered by the gas reduction process ($Al_2O_3 + NiO + CO = Al_2O_3 + Ni + CO_2$) (Fig. 6(a)), at higher magnification, it can be seen that there exists an amorphous material between the nickel inclusions and the alumina grains; EELS spectra (Fig. 6(b)) identify the film as amorphous carbon. The

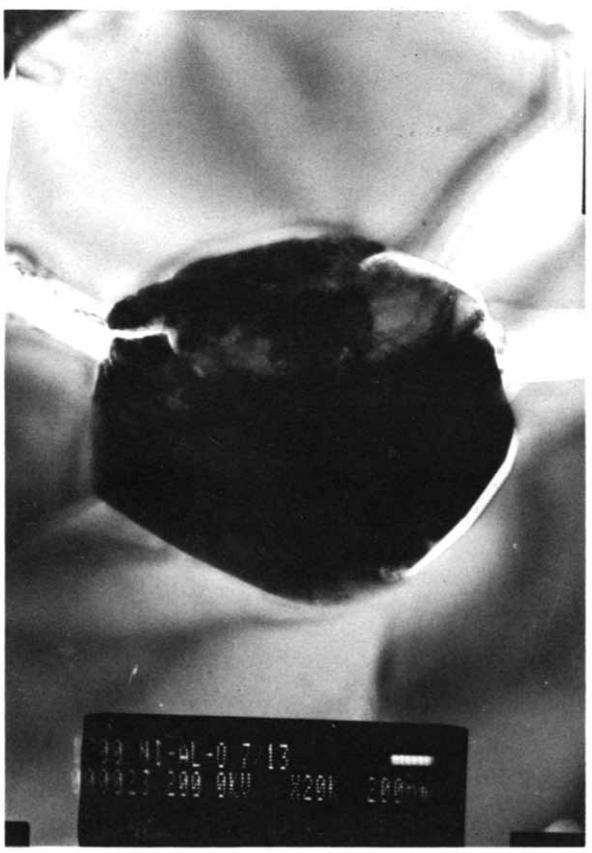

Fig. 5. Bridging nickel particle observed in the composite prepared by the gas reduction process. Note the debonding at the interface.

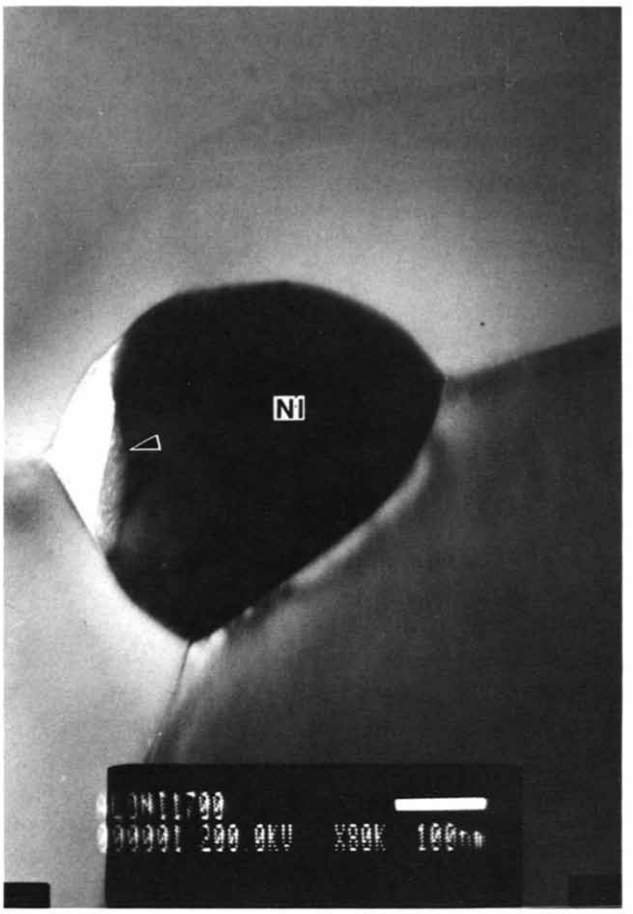

(a)

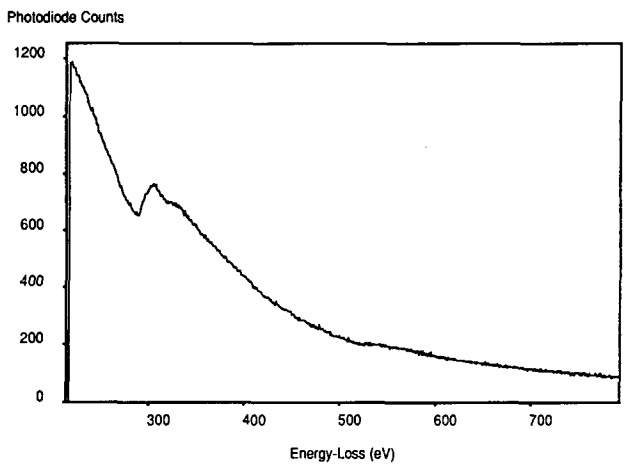

(b)

Fig. 6. (a) TEM micrograph for the sample prepared by the gas-reduction process, and (b) EELS spectrum from the carbon film region indicated by the arrow.

amorphous region is normally located at triple grain junctions. It was observed that pores are often associated with the amorphous carbon film, but some triple grain junctions are fully occupied with the amorphous carbon phase.

In reaction-sintered samples no such amorphous carbon layers have been observed; however, graphite inclusions within the nickel particles are often observed (Fig. 7(a)). The graphite inclusion is identified by electron diffraction, EELS and EDS (not shown) spectra, Fig. 7(b). No specific orientation

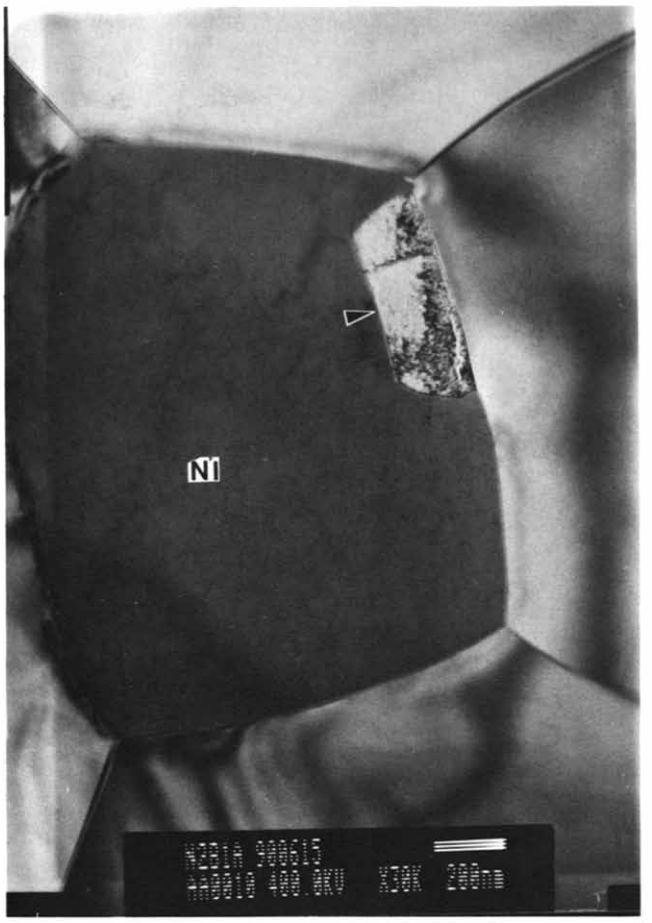

(a)

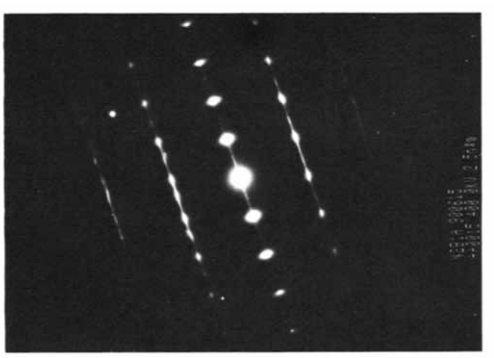

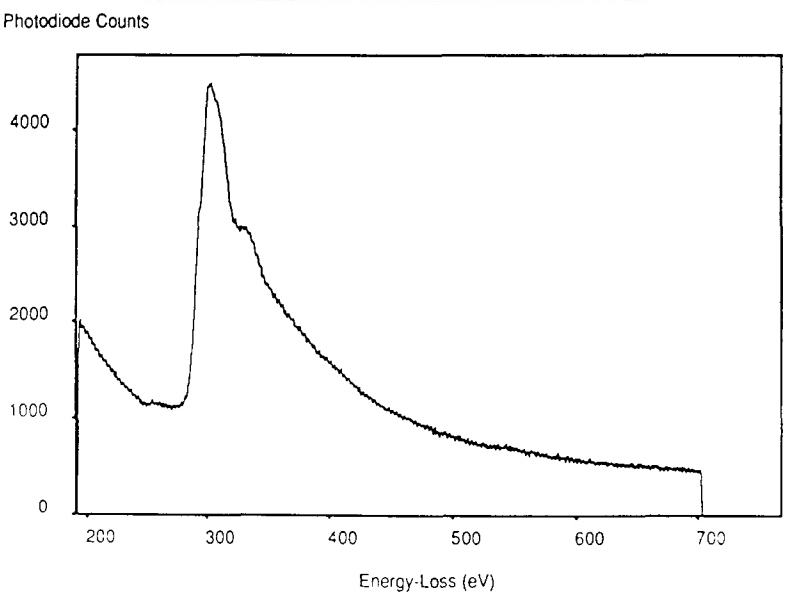

(b)

Fig. 7. (a) TEM micrograph from the sample prepared by the reactive sintering process, and (b) electron diffraction pattern and EELS spectrum from the graphite phase indicated by the arrow.

of the graphite phase with the alumina and/or nickel can be identified. Also, it is noted that all observed graphite inclusions are located at the interface between nickel and alumina, but within the nickel particles. The carbon content within the nickel inclusions prepared by the two processes has also been analysed by EELS technique. The carbon content is below the detection limits, < 1 wt%, of the technique.

4 Discussion

The difference of the interfaces prepared by the two processes lies mainly in the type and the location of carbon observed. The sintering atmosphere applied is virtually carbon monoxide. This atmosphere is generated by the graphite powder bed, as the reaction, $2C + O_2 = 2CO$, is active above 600°C.[10] At high temperature, carbon is dissolved in nickel. The solubility of carbon in solid and liquid nickel is shown in Fig. 8.[12] Owing to the different solubilities, carbon can be precipitated out on cooling, particularly as the nickel is solidified. The form of the precipitate, similar to the case of nickel–carbon alloy,[13] depends strongly on the process employed.

From Fig. 1, it is clear that the reaction heat between aluminium and nickel oxide is high in the reactive sintering case. This could contribute to the bigger inclusion size observed in Fig. 3. Since the solubility of carbon in nickel is increased at high temperature and the composites prepared by reactive sintering reach a much higher temperature (adiabatic temperature for the composition B1 is approximately 2527°C[10,14]) over a very short time period, excess carbon is dissolved in the nickel, then precipitated out as graphite inclusions in the nickel melt during cooling.

In the case of the composite prepared by the gas reduction process, the reduction of nickel oxide is almost complete at 1500°C.[5] No spinel is observed at the interface. During the late stage of sintering, the carbon monoxide is enclosed in the isolated pores. Three factors may contribute to the deposition of carbon on the pore surface: the first is the pressure increase due to the shrinkage of the pores; the second is the temperature decrease during cooling; the third is the precipitation of carbon from the nickel particles. While observing the pure alumina specimen sintered in the same environment, no amorphous layer at the pore surface is observed. The third factor is therefore the most likely reason for the amorphous layer observed in the samples prepared by the gas reduction process.

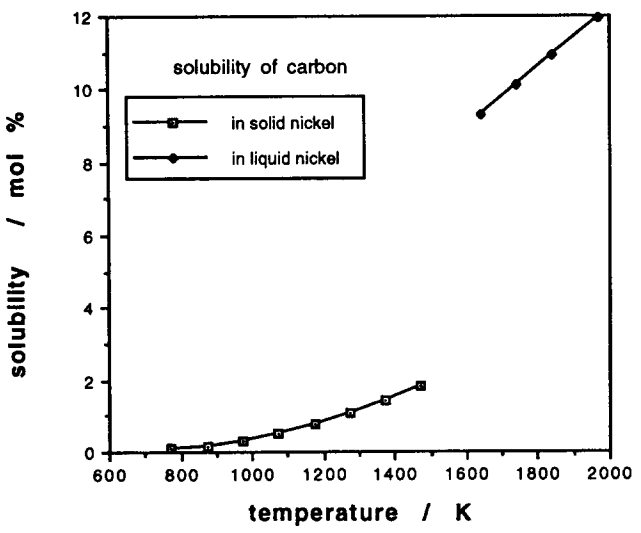

Fig. 8. The solubility of carbon in nickel as a function of temperature.

Bonding (or debonding) between the ductile phase and the ceramic matrix has a significant influence on the toughness of the composites. Ashby *et al.*[7] have shown that the toughness can be increased by several fold with increasing debonding. In the present work, the specimens prepared by gas reduction process show higher toughness than those prepared by the reactive sintering process, i.e. 5·0 versus 3·6 MPa $m^{0.5}$ at similar metal content. The conditions for the composites with similar nickel content are shown in Table 1. Due to there being no detectable carbon within the nickel inclusions prepared by the two processes, the elastic modulus and yield stress of nickel inclusions are assumed to be the same. From Table 1 and eqn (2), the value of C can thus be calculated, giving 0·2 for the composite prepared by reactive sintering, and 1·6 for the composite prepared by gas reduction. Notwithstanding the approximations involved, these values demonstrate the importance of interface character on the toughening of these ceramic–metal composites.

5 Summary

The interface between nickel and alumina in alumina/nickel composites is investigated. Due to the sintering atmosphere employed, carbon is dissolved in the nickel particles during sintering. For the composites prepared by the gas reduction process amorphous carbon is formed at the interface. Those prepared by reaction between aluminium and nickel oxide reach high temperature during processing and excess carbon is thus dissolved in the nickel, yielding graphite inclusions during cooling. The different resulting interfacial characteristics lead to different degrees of toughness enhancement.

Acknowledgment

The authors would like to thank Dr T. Y. Chu and Mr J. M. Liang for their technical help.

References

1. Simpon, L. A. & Wasylyshyn, A., Fracture energy of Al_2O_3 containing Mo-fibres. *J. Am. Ceram. Soc.*, **54** (1971) 56.
2. Hing, P. & Grove, G. W., The microstructure and fracture properties of MgO crystals containing a dispersed phase. *J. Mater. Sci.*, **7** (1972) 422.
3. Krstic, V. V., Nicholson, P. S. & Hoagland, R. G., Toughening of glasses by metallic particles. *J. Am. Ceram. Soc.*, **64** (1981) 499.
4. de With, G. & Corbijn, A. J., Metal fibre reinforced hydroxyapatite ceramics. *J. Mater. Sci.*, **24** (1989) 1411.
5. Tuan, W. H. & Brook, R. J., The toughening of alumina with nickel inclusions. *J. Eur. Ceram. Soc.*, **6** (1990) 31.
6. Flinn, B. D., Ruehle, M. & Evans, A. G., Toughening in composites of Al_2O_3 reinforced with Al. *Acta Metall.*, **37** (1989) 3001.
7. Ashby, A. F., Blunt, F. J. & Bannister, M., Flow characteristics of highly constrained metal wires. *Acta Metall.*, **37** (1989) 1847.
8. Bannister, M. & Ashby, M. F., The deformation and fracture of constrained metal sheets. *Acta Metall.*, **39** (1991) 2575.
9. Tuan, W. H. & Brook, R. J., Reactive sintering of Al_2O_3/Ni composites. *Brit. Ceram. Proc.*, **46** (1990) 335.
10. SGTE (Scientific Group Thermodata Europe) Substance Data Files, Version May 1987, Thermodata GmbH, Grenoble University, St. Martin d'Heres, France (1987).
11. Lawn, B. R., Evans, A. G. & Marshall, D. B., Elastic/plastic indentation damage in ceramics: The median/radial crack systems. *J. Am. Ceram. Soc.*, **63** (1984) 574.
12. Hoerz, G., Speck, H., Hehn, W., Formm, E. & Jehn, H., *Physics Data, Gases and carbon in metals*. Max-Planck Institute Stuttgart, Germany (1983).
13. Nemoto, M., Onisawa, K. & Suto, H., Precipitation of graphite and nickel carbide in a nickel-1·8 at% carbon alloy. *Trans. JIM*, **18** (1977) 331.
14. Munir, Z. A., Synthesis of high temperature materials by self-propagating combustion methods. *Am. Ceram. Soc. Bull.*, **67** (1988) 342.